Environmental Science
Processes & Impacts

Accepted Manuscript

ROYAL SOCIETY OF CHEMISTRY

rsc.li/process-impacts

Environmental impact

The on-water remote monitoring robotic system estimates the georeferenced distribution of cyanobacteria blooms avoiding physical damage on Anabaena sp. cyanobacteria colonies, which would provide an impact on current processes for monitoring, as well as the environmental studio of algae blooms and other benthos in the sublittoral zone to prevent possible physical damage of direct observation.

Journal Name

ARTICLE

On-water remote monitoring robotic system for estimating patch coverage of *Anabaena* sp. filaments in shallow water

Received 00th January 20xx,
Accepted 00th January 20xx

DOI: 10.1039/x0xx00000x

www.rsc.org/

E. Romero-Vivas,[a] F. D. Von Borstel,[a] C. J. Pérez-Estrada,[a] D. Torres-Ariño,[b] J. F. Villa-Medina[a] and J. Gutiérrez[a-c]

An on-water remote monitoring robotic system was developed for indirectly estimating relative density of marine cyanobacteria blooms at the subtidal sandy-rocky beach in Balandra Cove, Baja California Sur, Mexico. The system is based on an unmanned surface vehicle to gather underwater videos of the seafloor for avoiding physical damage on *Anabaena* sp. cyanobacteria colonies, which grow in tufts of filaments weakly attached to rocks, seagrass, and macroalgae. An on-axis image stabilization mechanism was developed to support a camcorder and minimize wave perturbation while recording underwater digital images of the seafloor. Color image processing algorithms were applied to estimate patch coverage area and density, since *Anabaena* sp. filaments exhibit a characteristic green tone. Results of field tests showed the feasibility of the robotic system to estimate relative density, distribution, and coverage area of cyanobacteria blooms, preventing possible impact of direct observation. The robotic system could also be used on surveys of other benthos in the sublittoral zone.

Introduction

Automated systems, equipped with actuators, sensors, and tools, are required to navigate and perform repetitive, dirty, and even dangerous tasks for a wide variety of applications. Mobile robotic systems have been deployed for mapping, remote sensing, sampling, monitoring, and surveying[1].

Survey methods that map nearshore vegetation can be categorized as: (1) physical, (2) off-water remote, and (3) on-water remote. Physical methods include direct observation and measurement by divers or beach walkers. It is always the approach recommended for preliminary surveys, but it requires labor-intensive fieldwork. Off-water remote sensing methods interpret aerial photography or satellite imagery, aided by computer algorithms. Extended areas can be surveyed with less field labor, but light absorption and reflectivity of water, water clarity, resolution of the images, and the properties of the image-collecting equipment limit the methods. These approaches, especially aerial photography, are expensive. On-water remote sensing methods interpret georeferenced underwater video or hydro-acoustic images that can provide precise mapping of moderately large areas, precise identification of vegetation, density, and general ecosystem stability or instability[2–6].

Georeferenced mapping of nearshore vegetation in very shallow water bodies is useful when boat-based surveys are unfeasible. This requires careful selection of survey methods, since direct observation and measurement by divers might have a strong impact on delicate filaments of algae that can be easily detached from the bottom. This problem calls for the use of novel on-water remote sensing solutions, such as the use of unmanned vehicles that must navigate with a strategy to minimize the effects of perturbation. New technologies and navigation strategies make possible vehicles with certain autonomy and data processing capabilities reducing operational costs with respect to manned vehicles[1, 7]. Potential applications for these robots in biological research include exploration, acquisition of physicochemical data, density estimation of different benthos, or even to monitor habitat changes by video recordings or photography.

Although there are approaches that use unmanned surface vehicles (USVs)[8–10], unmanned underwater vehicles (UUVs)[11, 12], or combine unmanned vehicles and off-water remotely sensed images (aerial and satellite imagery)[13, 14], georeferenced on-water remote image systems that use USVs in shallow water are uncommon.

The USVs can either be remote controlled or autonomous robots that contain their own on-board power and self-propelled while accomplishing an assigned task on the surface of water[15–17]. Research in this area is mainly focused on the use of microscopy and fluorometry for planktonic (free-floating) microalgae[18–20], rather than on filaments attached to the bottom in shallow water.

[a] Engineering Group, Centro de Investigaciones Biológicas del Noroeste S.C. La Paz, BCS 23000, México.
[b] Universidad del Mar Cd. Universitaria, Distrito de San Pedro Pochutla, Oaxaca 70902, México.
[c] Corresponding author, Email:joaquing04@cibnor.mx.

Cyanobacteria massively proliferate in freshwater, brackish water, and coastal marine ecosystems. Blooms of some toxic species can cause death of aquatic organisms and even human beings. Environmental and anthropogenic factors might enhance bloom formations[21–25]. To identify possible health and ecological risks due to marine cyanobacterial blooms, it is important to monitor its density, distribution, coverage area, and physical-chemical factors that are stimulating these blooms.

This article describes the use of a georeferenced USV that was designed for on-water remote sensing of cyanobacteria tufts in very shallow waters (less than 1 m) through process of underwater color images to estimate patch coverage area and relative density.

On-water Remote Monitoring Robotic System

The robotic system (Fig. 1) consists of an USV able to travel systematic paths based on data from a GPS and an electronic compass or through a control panel to operate the vehicle, and a waterproof video camera mounted at the bottom of the robot, using an on-axis image stabilization mechanism to minimize effects of surface wave motion. Data from the camera is analyzed, using color image processing algorithms to quantify the relative density of cyanobacteria blooms. Patch coverage is determined by the positions of the georeferenced images, in which a certain density threshold is surpassed. Water chemistry measurements of ammonia, nitrate, temperature, and conductivity can be simultaneously recorded with a sonde attached to the USV keel.

Unmanned surface vehicle

The USV (Fig. 2) was made of rigid polyvinyl chloride (PVC) plastic with a torpedo hull profile, 1.2 m long, 0.12 m diameter, and weighing 12 kg, including the payload. Two DC motors at 12 V and 1.75 A provide a differential steering, each one has a three blades brass propeller and is located at port and starboard, respectively. Endurance of two hours is provided by two 12 V and 8 A-h sealed rechargeable batteries for motors and other battery of 12 V and 4 A-h for the sensing, communicating, and computing devices, which are housed in a removable acrylic cylinder along with the electronic circuitry. A sonde to acquire water physicochemical data and a camera–stabilizer are attached to the keel of the USV.

The USV can be operated in an autonomous mode with programed paths based on waypoint setup of distances (d_w) and heading angles (θ_w), or in a teleoperated mode. In both cases, a personal digital assistant (PDA) through a radio frequency (RF) modem provides a control panel for programming the sequence of waypoints or commanding the vehicle, and receiving feedback of the current position (latitude, longitude, and heading), time (UTC), and tilt angles (roll and pitch). Fig. 3 shows a screen of the graphical user interface (GUI) to drive the vehicle.

The USV control architecture has three controller modules: main, sensor, and actuator. The main controller runs the

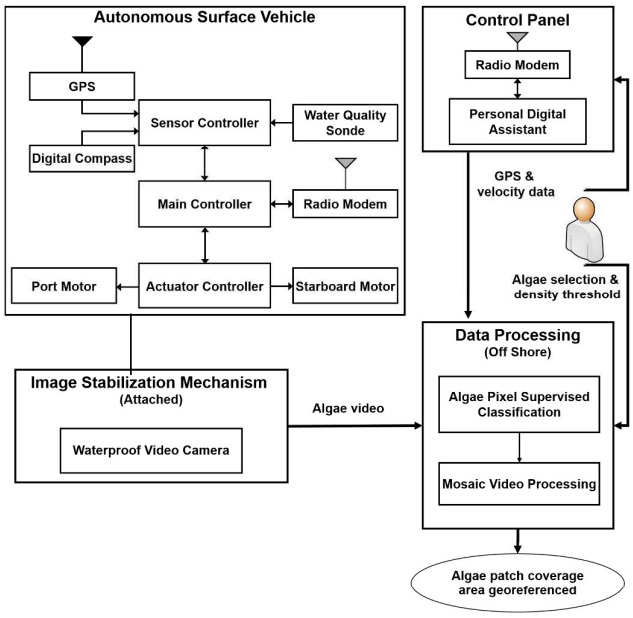

Fig. 1 On-water remote-sensing robotic system: Unmanned surface vehicle, control panel, image stabilization mechanism, and data processing.

algorithms for onboard control with raw sensor data processing, receives user commands, and manages the external communication with the control panel via a full-duplex RF link.

This controller was implemented on an RCM4110 microprocessor core with algorithms programmed in Dynamic C. The sensor controller (running on a second RCM4110 microprocessor) processes navigation data from an onboard global positioning system (GPS NMEA compliant, updated at 1 Hz rate), an electronic compass (updated at 8 Hz rate), and a water sensing sonde YSI model 6920. The GPS is a Garmin 15xL receiver module with a 48 dBm high-gain antenna to provide latitude, longitude, and time through an asynchronous serial

Fig. 2 The USV is equipped with a water quality sonde and electronic components; the latter were housed in a sealed acrylic container.

Fig. 3 The control panel contains a personal digital assistant, a radio modem, a battery, and a graphical user interface that is used to operate the USV.

port at 38400 bauds. A Honeywell HMR3300 digital compass provides heading reference with accuracy of 1° RMS, a resolution of 0.1°, and tilt compensation up to ±60°. The actuator controller receives from the main controller the commands to drive the propulsion motors. This controller is a custom-made, printed circuit board based on a PIC16F690 20-pin flash microcontroller, opto-isolators, and two MC33887 full H-Bridges to control motor power and direction.

The control panel was implemented in C# programming language in a HP iPaq hx2790 PDA with the Windows Mobile™ 5 running in an Intel® PXA270 processor at 624 MHz and a 3.5" transflective 320 × 240 pixel display. Data between the main controller and the control panel is exchanged using XTend® 900 MHz OEM RF half-duplex modems, programmed at 115.2 Kbps data rate with a line-of-sight range up to 1 miles.

The shape of the USV was based on the Myring[26] hull profile equations to minimize the drag coefficient with respect to the ratio of body length and diameter and operate in shallow water at environmental condition in Beaufort scale 1 (wind speed interval of 1.1–5.5 km/h) and wave height up to 0.2 m. The buoyancy force estimated was 12 N, assuming 87 % of the hull was immersed in seawater.

The capacity of the differential motors (F_T) was estimated, based on the drag equation, described as:

$$F_T = F_D = \frac{1}{2}\rho v^2 A_h C_D \qquad (1)$$

where F_D is the drag force acting on the hull, C_D is the drag coefficient, A_h is the maximum cross-sectional area of the hull, v is the USV forward speed, and ρ is the seawater density (1025 kg/m^3). Assuming the immersed area of the hull, the forward speed of 1.5 m/s, and the drag coefficient equal to 0.7, a drag force of 7.9 N is required. Also, considering a total efficiency reduced to 0.3, including the motor, propeller, and mechanical efficiencies, the estimated power capacity of 40 W is provided by the two motors selected.

Image stabilization

A video camera attached to the USV would swing with surface wave motion; therefore, image stabilization is required to reduce this movement on the video. The methods used to stabilize the video image include external elements that steady the camera and mechanical actuators inside the camera to adjust the optical path[27]. Modern cameras include image stabilization mechanisms, most of them active, which have been mainly designed for stabilization on the focal plane, compensating for small linear camera movements for close-ups and macro-photography, or in more expensive models, to compensate for rotation of the camera for distant subjects. Also, these systems are designed to reduce hand shaking and body movement associated with regular frequency movement and small movement amplitudes[28].

There are several efforts to stabilize the camera on remotely operated submersible vehicles[29]. Most of them use active control systems, mostly to correct linear movements in the focal plane. The problem that our approach faced differs from those studies in several respects. First, the downward facing video camera needs to be stabilized on the horizontal axis, not in the focal plane, which is the case for cameras facing frontwards. Second, the platform is on the surface, moving with the waves, but the camera is immersed in the water at a specific depth. In most cases, vehicle and camera are submerged. Third, the vehicle is driven by relatively high amplitude–low frequency waves compared with on board camera systems with must adjust to low amplitude–higher frequencies produced by hand shaking. For this application, an image stabilization mechanism was designed.

The mechanism for image stabilization is built of lightweight plastic pieces and rubber bands. The prototype and analytical model of the system is shown in Fig. 4. This arrangement of passive links and a hydrodynamic base reduces roll, yaw, and pitch movements of the camera, while the USV covers the assigned path.

The stabilization mechanism is allocated and locked to the USV keel; whereas the camera is mounted into the hydrodynamic base. The system acts as a mechanical, low pass filter that can be modeled as a damped oscillator excited by a periodic

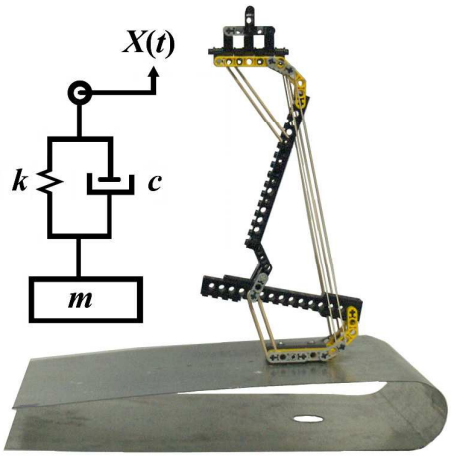

Fig. 4 Image stabilization mechanism and its analytical model.

external force applied to the mass[30]. The surface waves move the USV acting as a periodic external force $X(t)$, while the plastic bands provide the stiffness of the spring k in the model. The damping component c is provided by the surface of the hydrodynamic base acting on the water column. The waterproof camera adds mass m to the system. The image stabilization mechanism is designed to decouple the vertical movement of the video camera from the movements of the USV that are produced by moderate sea waves.

Image processing for assessment of cyanobacteria

The area covered by the cyanobacteria filaments is in constant change as the growing conditions change. Furthermore, the boundary of the patch coverage is undefined because isolated filaments at the fringe could spread and grow (or be detached) in any direction. However, a boundary could be practically defined by setting a threshold on the density of the filaments. Consequently, to estimate the patch coverage area through video processing, it is necessary to identify the filaments in each photogram, compute the relative density in each image, and select those georeferenced images that contain a density value above the selected threshold.

Cyanobacteria filaments exhibit a characteristic green tone, and therefore color image processing algorithms can be applied to the underwater digital images to differentiate them. The algorithm to identify the cyanobacteria by color has been described within the context of identification of structures in histology[31] and lizard color classification[32], and is briefly described below and shown in Fig. 5.

Algae pixel supervised classification. After a survey on the study area, the video file (.mpg format) is decomposed in n images (n video frames). A training set is comprised of 50 images selected randomly. A biologist identifies the algae of interest in each frame (bearing into account other features besides color, like shape and attaching substrate) and selects certain areas within the algae using a GUI. The images of the cyanobacteria filaments comprise a range of tones due to biological and physical factors (such as illumination and suspended particles). That variability is captured within the samples identified by the expert as the algae of interest, and registered as a matrix of RGB color values of the pixels within the areas selected. When all training images are processed, a cluster is calculated from the RGB color range matrix assuming a Gaussian mixture distribution, and a centroid and boundary limit are defined. It is important to notice that parameters obtained from training this set are valid only for that specific survey.

Once a centroid and boundary limits are obtained from the training set, the complete video is processed to identify cyanobacteria filaments in each image. RGB values are obtained from each pixel within an image and its Mahalanobis distance to the centroid computed, if this distance is within the boundary limit previously defined the pixel retains its RGB color value, otherwise it is set to color white.

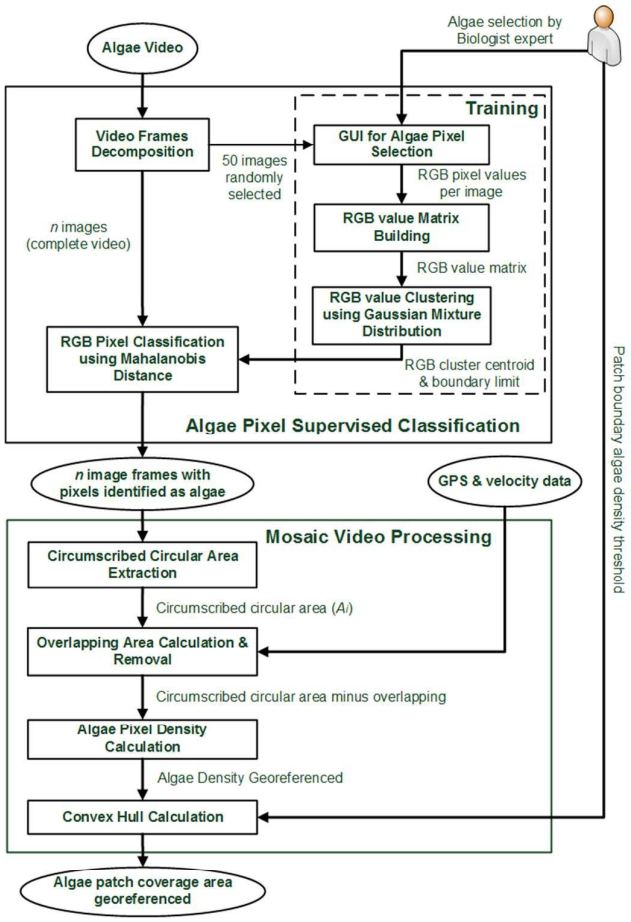

Fig. 5 Procedure to compute relative density and patch coverage area.

Each frame is processed in this manner and consequently only the algae of interest remains in the picture over a white background.

Mosaic video processing. By counting the number of pixels in an image that are defined as *Anabaena* sp. out of the total, relative cyanobacteria density can obtained for each frame, but further processing is required to account for overlap between frames. As described previously, video taken of the cyanobacteria patch is georeferenced every second. All images taken between GPS position marks are considered for the density estimates, since the video frame rate is higher than the position refresh rate. Moreover, although a rectangle is obtained for each video frame, a circumscribed circular area is considered because the image frames can be superimposed in any direction, depending on the heading of the USV and the camera.

Fig. 6 illustrates this concept. Overlapping circles represent the video frames taken, with the overlap being proportional to the velocity of the USV. At the bottom right, a couple of circles represent contiguous frames in the video. To avoid overestimating the cyanobacteria content in consecutive

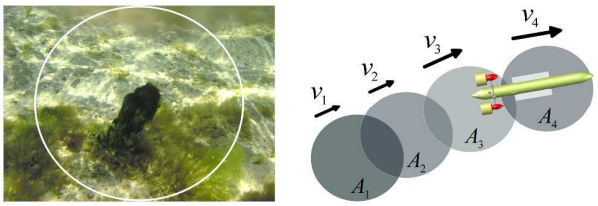

Fig. 6 Circumscribed circular area defined for each photogram and mosaic video processing.

frames, the intersection has to be subtracted from the result of adding both frame areas (mosaic video processing).

During the trajectory, depending on the USV velocity, the superimposed circular area (A) between image frames can be calculated by fixing the A_i centroid and moving the A_i + 1 centroid a distance obtained by dividing the velocity data between the image frames rate per second. The centroid movement is calculated over the x-axis. Then, the sum of both areas, minus its intersection, is calculated and this procedure continues until a new GPS position.

Using this mosaic video processing, algal density can be found for overlapping frames at each GPS position. A threshold can be established to select those positions that have a certain percentage of algal density. Those positions, labeled as inner points, have georeferenced coordinates and therefore a convex hull can be computed to estimate the boundary and patch coverage area.

Monitoring Robotic System Implementation

Each element of the robotic system was tested and evaluated in a study area. First, the USV had to be able to navigate over the area covered by the patches under certain current and surface conditions and gather information, following programmed paths or teleoperated despite surface waves, winds, and currents had to be assessed. Second, the image stabilization mechanism had to compensate for the movements of the USV caused by surface waves or at least be minimized to be able to obtain useful video images for analyses. Third, the algorithms designed for detecting and estimating the density of the algae *Anabaena* sp. should be able to differentiate this colonial organism from other cyanobacteria in the area.

USV performance

The USV used differential driving to control the vehicle motion. In autonomous mode, the paths to follow were composed of waypoints that involved a distance to travel (d_w) with a heading angle (θ_w) to reach a destination.

The waypoint-based path can be recorded in the main controller or generated and transmitted by means of the control panel, starting on the current location of the USV. Each waypoint ($d_w(k)$, $\theta_w(k)$) was converted to points ($x(k)$, $y(k)$) in the Euclidean plane by the onboard algorithm, and a proportional controller is used to follow the heading by driving the differential motors. The GPS and digital compass

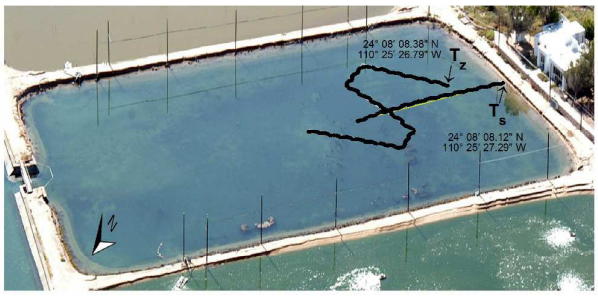

Fig. 7 Straight and zigzag paths performanced by the USV, superimposed on an aerial photograph of an aquaculture pond.

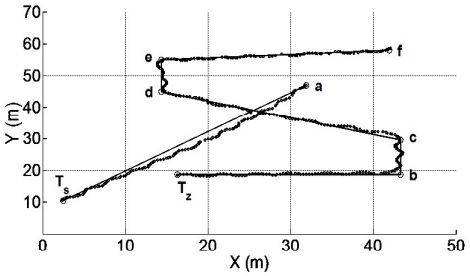

Fig. 8 Results of programmed straightforward (Ts) and zigzag (Tz) paths performanced by the USV in an aquaculture pond: USV locations (dotted lines) and programmed waypoints (solid lines).

information were used to estimate current position, $x_e(k)$ and $y_e(k)$, and orientation, $\theta_e(k)$. The criterion to identify if the waypoint has been reached was defined by Euclidean distance, for which the threshold position ε must be less than the vehicle length (ε < 1.2 m): If the criterion was satisfied, the USV navigate toward the next waypoint on the path.

To validate the control algorithm, the USV was programmed to track waypoint-based paths in an aquaculture pond located at 24° 08′ 8.12′′ N and 110° 25′ 27.9′′ W, under light wind speed that corresponds to the scale of Beaufort 1. Figs. 7 and 8 show the results for a straightforward path, starting at the waypoint T_s and finishing at point a; and a zigzag path, starting on the waypoint Tz and passing by the b, c, d, e, and f points. The USV location is indicated with dotted lines, and solid ones outline the waypoint-based paths. The experimental paths show that the approach of waypoint tracking, implemented in the USV, was successfully achieved.

Study area

The shallow Balandra Cove (24° 20′ N, 110° 19′ W) along Bahía of La Paz has a shoreline that varies from mangrove, gentle sandy beaches, and rocky reef and headlands. The sandy bottom of the cove is an important natural asset for bottom dwelling; also the cove is one of the major recreation areas for residents and visitors to La Paz. At low tide, the sandy bottom of the cove is very shallow: semi-diurnal high tides range from 1–1.5 m. Water temperature ranges from 20–31 °C, depending on season.

The filaments of cyanobacteria were mainly composed of *Anabaena* sp.[33], which are usually found as straight, uniserial,

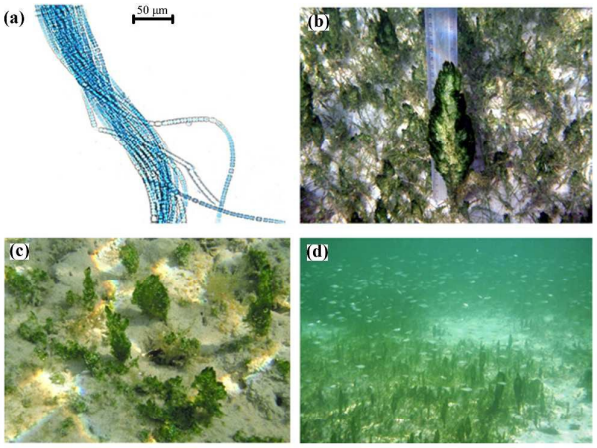

Fig. 9 *Anabaena* sp. Filament structure (a), filaments (b), substrate (c), and patches (d).

unbranched structures of vegetative cells, and heterocysts (Fig. 9a). The filaments are usually abundant, arranged in parallel strands or tangled screw-like spiral filaments whose size varies from a few millimeters to about 20 cm (Fig. 9b). Filaments are found in the subtidal zone where the bottom is a sandy and rocky beach ranging from 0.30–1 m (Figs. 9c, 9d).

To protect the cyanobacterial colonies that were found at 0.70 m depth in the study area, the USV was operated remotely in the area of study to gather the digital images. Additionally, the wind reached 2 of the Beaufort scale that produces waves up to 0.5 m height.

The image stabilization mechanism

To analyze the performance of the stabilization mechanism a submarine B&W video camera (SWL-UWC Swann Underwater Cam) took the profile of the USV and the camera stabilizer mechanism (15 fps @ 512 x 304 pixels) at the seacoast near to the cyanobacterial location.

A segment of 25 seconds of video in which the USV is freely moved by the sea waves (Beaufort 1) was selected for analysis. In each frame, 3 points of the image were visually selected: two points to define the USV profile line and a third point at the support wing holding the camera. A Matlab® application was developed to extract the relative coordinates of these marks. Fig. 10 shows one of the frames for analysis and the 3 points selected: Stern, bow and camera, respectively.

Taking the coordinates in each frame as a time signal representing the relative movement of the USV and the camera, the effect of the stabilizer on the vertical axis was analyzed. Fig. 11 shows a boxplot of the displacement for each point. On each box, the central mark is the median, the edges of the box are the 25th and 75th percentiles, and the whiskers extend to the most extreme data points not considered outliers. The camera mark clearly shows a similar median to the stern mark but much smaller displacements, even for the most extreme movements. Fig. 12 shows a frequency analysis. The stabilization mechanism effectively reduces the movement for the main frequency peak of the USV, which has amplitude of 0.13 m and 0.11 m (Stern and Bow) to only 0.026 m at the camera position (Camera). The system effectively decouples the movement of the camera from the motion of the USV due to the sea waves.

The algorithms for detecting *Anabaena* sp.

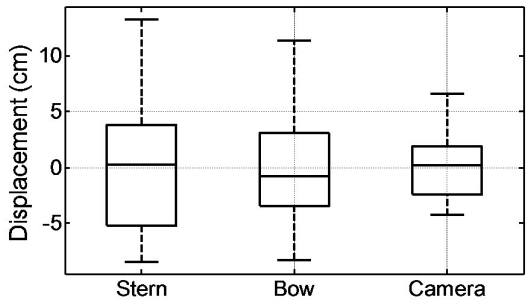

Fig. 11 Performance of stabilization mechanism on the USV.

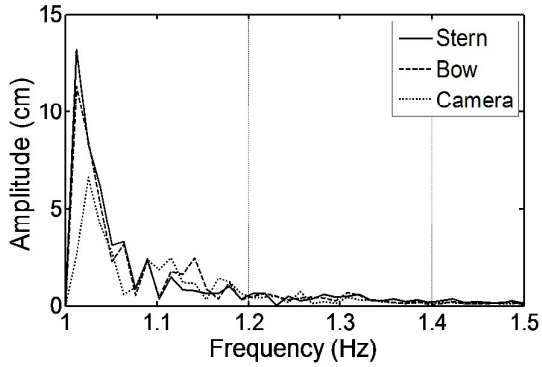

Fig. 12 Performance of the stabilization mechanism: Amplitude vs frequency for the stern, bow, and camera.

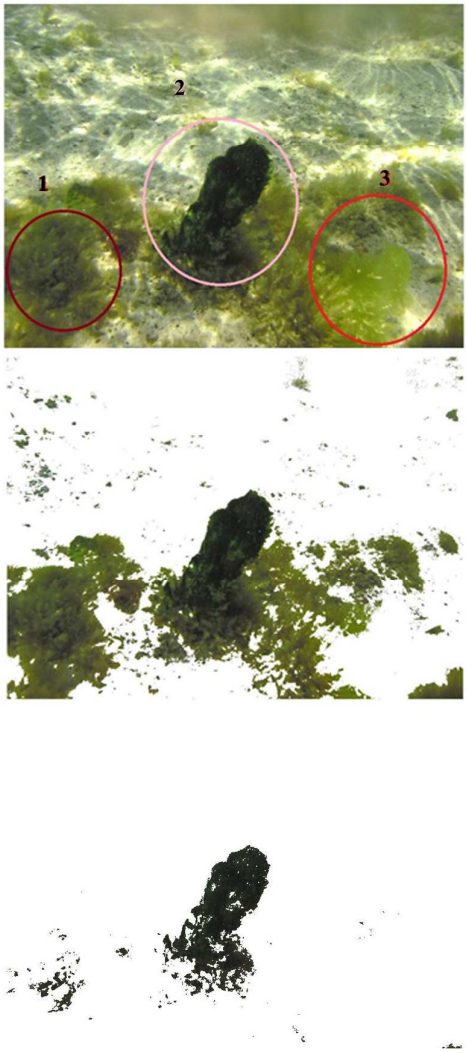

Fig. 13 Cyanobacteria detection. Top, three algae: 1) *Acanthophora spicifera* (Rhodophyta); 2) *Anabaena* sp. (Nostocaceae), and 3) *Ulva* sp. (Chlorophyta). Middle, algae: *Acanthophora spicifera* and *Anabaena* sp. Bottom, only *Anabaena* sp.

Cyanobacteria filaments were identified in a set of 50 randomly chosen images, and the algorithm described earlier was applied to each video frame. Fig. 13 shows a sample image, where two types of algae and one cyanobacterium can be identified: *Acanthophora spicifera* (1) that is a species of marine red algae in the family Rhodomelaceae, *Anabaena* sp. (2), and *Ulva* sp. (3), which is a species of green algae in the family Ulvaceae. The middle image shows the algorithm applied to identify only *Acanthophora* and *Anabaena* sp. Notice that *Ulva* sp. has been removed, as well as the sandy substrate. The image at the bottom shows the results for identification of *Anabaena* sp. The algorithm proves to be able to distinguish specific species of algae despite their similar green color.

Estimating relative density and patch coverage area

The robot in the area of interest performed several trajectories randomly. A threshold of 66% was selected for the density value that defines patch boundaries. Fig. 14 shows the paths

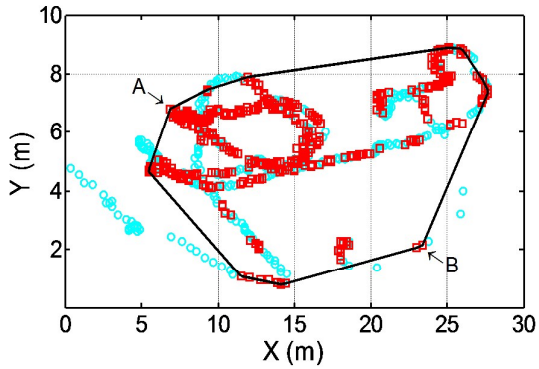

Fig. 14 Patch coverage area (124 m^2) for a relative density of 66 %.

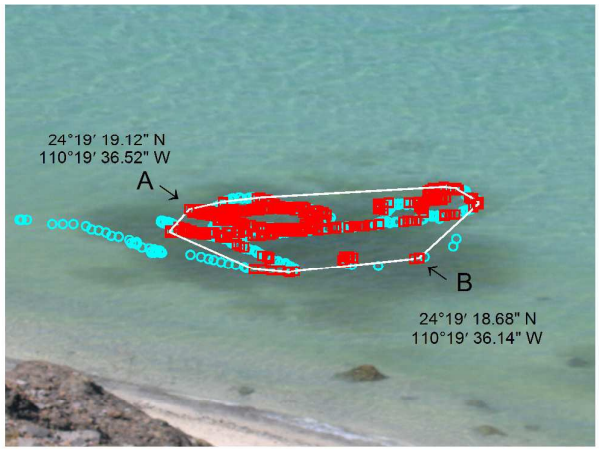

Fig. 15 Patch coverage area for a relative density of 66 % superimposed on an aerial photograph of the study area.

followed by the USV. Blue dots represent the georeferenced positions, where the relative density estimates are below that threshold. The red squares represent the positions with density above the threshold. A convex hull, which represents the boundary of the patch, is drawn by a polygon formed by the outer red squares. Fig. 15 shows the paths and computed boundaries superimposed over the patch. Points A and B and their GPS coordinates are shown for reference. The aerial view shows the patch as a brown shadow with darker tones that signal higher density, but this is not easily quantified from the image. The robotic system provides a closer estimate of the density boundaries of the patch, but only as long as the paths cover the whole surface.

Conclusions

The georeferenced unmanned surface vehicle and image processing system is a reliable tool to acquire systematic data acquisition tasks. This system will be particularly useful to monitor and estimate distribution, abundance, and coverage area of algae, seagrass, or other benthos; providing useful information resource for environmental management programs. The video image processing algorithms provided precise identification of vegetation, density, and general health of the habitat. Since video images and acquired data are

stored digitally, it can be reviewed for post processing and easily transferred into GIS tools for later analysis, providing precise information with less effort, time, and cost.

The effectiveness of the underwater video camera system can be considerably reduced by water column turbidity. At high turbidity, resolution of the images greatly diminishes, as does the ability of laboratory investigators to interpret the imagery. Hence, a preliminary analysis of atmospheric and water quality conditions is recommended before initiating underwater recording video of benthic habitats.

Furthermore, this robotic system is a cost-effective alternative for on-water monitoring in shallow water; its cost is about units of thousands of dollars instead of tens of thousands of dollars for commercially-available systems.

Acknowledgements

We thank Jorge Cobos Anaya and Alfonso Alvarez for technical support in the construction of the USV and Salvador Lluch Sicard for his help in the design of the image stabilizer. Ira Fogel of CIBNOR provided editorial improvements. FOMIX CONACYT-Sinaloa (SIN-2005-C01-03) funded the USV development.

References

1 HA. Durrant-Whyte, *Critical review of the state-of-the-art in autonomous land vehicle systems and technology*, Technical Report SAND2001-3685, Sandia National Laboratories, 2001.

2 B.M. Sabol, R.E. Melton, Jr. R. Chamberlain, P. Doering and K. Haunter, Evaluation of a digital echo sounder system for detection of submersed aquatic vegetation, *Estuaries*, 2002, **25**(1), 133-141.

3 Ch. Fairbanks and J. Norris, *Whatcom County submerged: Aquatic vegetation survey methods*, NOOA Report, 2004.

4 4R.L. Miller, C.E.D. Castillo and B.A. McKee, *Remote sensing of coastal aquatic environments*, Kluwer Academics Publishers, Dordrecht, 2005.

5 F. Dahdouh-Guebas, E. Coppejans and D. Van Speybroeck, Remote sensing and zonation of seagrasses and algae along the Kenyan coast, *Hydrobiologia*, 1999, **400**, 63–73.

6 A. Ruiz-Verdú, S.G.H. Simis, C. de Hoyos, H.J. Gons and R. Peña-Martínez, An evaluation of algorithms for the remote sensing of cyanobacterial biomass, *Remote Sens. Environ*., 2008, **112**(11), 3996-4008.

7 C. Pêtrès, M.A. Romero-Ramirez and F. Plumet, A potential field approach for reactive navigation of autonomous sailboats, *Robot Auton. Syst*., 2012, **60**(12), 1520-1527.

8 K.H. Low, G. Podnar, S.B. Stancliff, J.M. Dolan and A. Elfes, *Robot Boats as a Mobile Aquatic Sensor Network*, International Conference on Information Processing in Sensor Networks (IPSN) Workshop on Sensor Networks for Earth and Space Science Applications: ESSA, April 2009.

9 A. Singh, M. Batalin, M. Stealey, B. Zhang, A. Dhariwal, B. Stauffer, S. Moorthi, C. Oberg, A. Pereira, V. Chen, Y. Lam, D. Caron, M. Hansen, W. Kaiser and G. Sukhatme, Human assisted robotic team campaigns for aquatic monitoring, *J. Field Robot*., 2007, **24**(11-12), 969-989.

10 Y. Kaizu, M. Iio, H. Yamada and N. Noguchi, Development of unmanned airboat for water-quality mapping, *Biosyst. Eng*., 2011, **109**(4), 338-347.

11 J. Das, J. Harvey, F. Py, H. Vathsangam, R. Graham, K. Rajan and G. Sukhatme, *Hierarchical Probabilistic Regression for AUV-based Adaptive Sampling of Marine Phenomena*, In IEEE International Conference on Robotics and Automation, May 2013.

12 S. Frolov, J. Bellingham, W. Anderson and G. Hine, *Wave Glider—A platform for persistent monitoring of algal blooms*, Oceans 19-22 Sept. 2011, 1-5.

13 S.C.Y. Leong, P. Tkalich and N.M. Patrikalakis, *Monitoring harmful algal blooms in Singapore: Developing a HABs observing system*, Oceans 21-24 May 2012, 1-5.

14 R.N. Smith, M. Schwager, S.L. Smith, B.H. Jones, D. Rus and G.S. Sukhatme, Persistent Ocean monitoring with underwater gliders: Adapting sampling resolution, *J Field Robot*., 2011, **28**(5): 714–741.

15 V. Bertram, *Unmanned surface vehicles - a survey*, Technical report, Cole Nationale Suprieure des Ingnieurs destudes et Techniques d'armement (ENSIETA), 2008.

16 JE. Manley, *Unmanned surface vehicles*, *15 years of development*, Oceans 15-18 Sept. 2008, 1 - 4.

17 M. Caccia, M. Bibuli, R. Bono and G. Bruzzone, Basic navigation, guidance and control of an unmanned surface vehicle, *Auton. Robots*, 2008, **25**(4), 349-365.

18 J. Das, K. Rajan, S. Frolov, F. Pyy, J. Ryany, D. Caron and G. Sukhatme, *Towards marine bloom trajectory prediction for AUV mission planning*, Robotics and Automation (ICRA), 2010 IEEE International Conference on 3-7 May 2010, 4784-4790.

19 K. Ishikawa, M. Kumagai and R.F. Walker, Application of autonomous underwater vehicle and image analysis for detecting the three-dimensional distribution of freshwater red tide Uroglena Americana Chrysophyceae, *J. Plankton Res*., 2005, **27**(1), 129–134.

20 A. Alum, B. Mobasher, A. Rashid and M. Abbaszadegan, Image analyses-based nondisruptive method to quantify algal growth on concrete surfaces, *J. Environ. Eng*., 2009, **135**(3), 185-190.

21 KG. Sellner, Physiology, ecology, and toxic properties of marine cyanobacteria blooms, *Limnol. Oceanogr*., 1997, **42**(5), 1089-1104.

22 B. Luděk, B. Pavel and M. Blahoslav, Toxins produced in cyanobacterial water blooms-toxicity and risks, *Interdiscip. Toxicol*. 2009, **2**(2), 36–41.

23 G.A. Codd, L.F. Morrison and J.S. Metcalf, Cyanobacterial toxins: risk management for health protection, *Toxicol. Appl. Pharmacol*., 2005, **203**, 264–272.

24 P. Coltelli, L. Barsanti, V. Evangelista, A.M. Frassanito and P. Gualtieri, Water monitoring: automated and real time identification and classification of algae using digital microscopy, *Environ. Sci.: Processes Impacts*, 2014, **16**(11), 2656-2665.

25 A. Zamyadi, S. Dorner, M. Ndong, D. Ellis, A. Bolduc, C. Bastien and M. Prevost, Application of in vivo measurements for the management of cyanobacteria breakthrough into drinking water treatment plants, *Environ. Sci.: Processes Impacts*, 2014, **16**(2), 313-323.

26 DF. Myring, A theoretical study of body drag in subcritical axisymmetric flow. *Aeronaut. Quart.*, 1976, **27**(3), 186–194.

27 R. Wotiz, Camera image stabilization, *Circuit Cellar*, 2012, **262**, 46-50.

28 D. Sachs, S. Nasiri and D. Goehl, Image stabilization technology overview,http://www.invensense.com/mems/gyro/documents/whitepapers/ImageStabilizationWhitepaper_051606.pdf, (accessed October 2014).

29 C. Braufaldi, P. Firoozfam and S. Negahdaripour, An integrated vision-based positioning system for video stabilization and accurate local navigation and terrain mapping, Oceans 2003 Proceedings, **2003**(5), 2567-2573.

30 S. Rao, *Mechanical vibrations*, Fifth Edition, Prentice Hall, Upper Saddle River, NJ, 2004.

31 C. Rodríguez-Jaramillo, M.A. Hurtado, E. Romero-Vivas, J.L. Ramírez, M. Manzano and E. Palacios, Gonadal development and histochemistry of the tropical oyster, Crassostera cortiziensis (Hertlein, 1951) during an annual reproductive cycle. *J. Shellfish Res*., 2008, **27**(59), 1-13.

32 VC. Meza López, Evaluación de la época reproductiva de la lagartija Aspidoscelis hyperythra mediante estudios hormonales y de coloración, Master Thesis, CIBNOR, 2011.

33 J. Komárek and K. Anagnostidis, Modern approach to the classification system of cyanophytes, 2 - Chroococcales. Arch. Hydrobiol/Algolog. Stud., 1986, 43, 157-226.